An investigation on VIV of a single 2D elastically-mounted cylinder with different mass ratios

Riccardo Pigazzini[1] · Giorgio Contento[1] · Simone Martini[1] · Mitja Morgut[1] · Thomas Puzzer[1]

Accepted: 30 October 2018

Abstract
The effect of the mass of a 2D elastically-mounted circular cylinder in cross-flow on its vortex-induced vibrations and on the related vortex shedding lift forces is analyzed via a single-degree-of-freedom multi-frequency model (sdof-mf). The mechanical system in question is characterized by low mass ratio, low structural damping and Reynolds number of order 10^4. The proposed sdof-mf model relies on the decomposition of the total hydrodynamic force in a inertia/drag force, conventionally associated with the cylinder motion in still fluid, and an additional lift force associated to pure vortex shedding. The lift force is assumed to be composed by not-Fourier-dependent harmonics; this constitutes the key point of the proposed sdof-mf model. The parameters of this model are determined via a parameter identification method based, in this case, on VIV data obtained via CFD. The simulations are carried out changing systematically the values of the mass ratio, within the range of engineering practice, and covering a wide range of flow regimes including lock-in conditions. The results from the application of the sdof-mf model highlight the large influence of the mass ratio on the response of the cylinder and on the vortex shedding lift force. The effects are clearly visible on the maximum amplitude at lock-in, on the range of incident flow velocity over which synchronization occurs, on ultra/sub harmonic behavior and phase lag of the cylinder motion, and finally on the magnitude and harmonic content of the lift force induced by pure vortex shedding.

Keywords VIV · sdof-mf model · Parameter Identification · Mass ratio

1 Introduction

Vortex-induced vibrations (VIV) occur when vortices shed by a blunt structure in steady (or unsteady) flow induce an oscillatory force on the structure, mostly in the direction perpendicular to the ambient flow. If the structure is free to move in this direction or is partially restrained by restoring/damping forces (moorings, structural stiffness, etc.), the body starts oscillating. The quasi-synchronization (lock-in) between vortex shedding frequency and natural frequency f_0 may occur; as a consequence, the structure undergoes near-resonance motions and large displacements are typically observed. Strong variations of the response amplitude with the speed of the incident flow U are found too, even if related to very small variations of the latter.

The typical behavior of the amplitude A of the motion of the body with increasing background flow speed U is characterized by: (1) an initial branch where A grows rapidly with U starting from very low values; (2) an upper branch where A reaches its max; (3) a lower branch where A is still large but with lower values, both upper and lower branches in quasi-synchronization conditions; (4) a desynchronization region where A tends towards low values.

The amplitude A of the motion of a smooth cylinder may be of the same order of the characteristic size of the body (commonly the cylinder diameter D), depending on several parameters, among others the Reynolds number Re, the non-dimensional background fluid velocity (reduced velocity U^*), the mass ratio (m^*), the stiffness of the restoring mechanism,

✉ Giorgio Contento
contento@units.it

Riccardo Pigazzini
riccardo.pigazzini@phd.units.it

Simone Martini
simone.martini@phd.units.it

Mitja Morgut
mmorgut@units.it

Thomas Puzzer
tpuzzer@units.it

[1] Department of Engineering and Architecture, University of Trieste, via A. Valerio 10, 34127 Trieste, Italy

the non-dimensional mechanical damping (damping ratio ζ) and combinations of the latter (for instance, the mass-damping parameter $m^*\zeta$). The subject has received huge consideration and a large amount of literature is available, covering many aspects of the problem. Among others, Bearman [1, 5], Govardhan and Williamson [2], Gabbai and Benaroya [3] and Williamson and Govardhan [4] have given very detailed reviews of VIV. For further insight on the topic, the reader is redirected to the above mentioned and to the following experimental and numerical works by Khalak and Williamson [6], Vikestad et al. [7], Norberg [8], Guilmineau and Queutey [9], Wanderley et al. [10], Wu et al. [11], Mittal and Mittal [12].

In their review, Williamson and Govardhan [4] have analyzed the effect of mass and damping ratios, according to a variety of existing data from the literature. They have shown how the mass ratio affects (1) the dominant frequency in synchronization conditions, (2) the maximum amplitude of motion in upper and lower branches of the response, and (3) the upper limit of U^* of the synchronization region.

Bahmani and Akbari [13] have analyzed the effect of mass and damping ratios via 2D simulations based on a vortex method. The Reynolds number used in that work is relatively low, of order of 10^2, the mass-damping parameter is quite high, always above 0.1, and the mass ratios are of order of 10^2. They confirmed the results known from the literature, showing that, in the conditions and within the parameters used, the non-dimensional amplitude response $A^* = A/D$ is always upwardly bounded by the conventional value of 0.6 and that there is no clear evidence of distinct upper and lower branches. They ascribe this effect to the low Reynolds number and mostly to the high mass-damping parameter.

Modir et al. [14] have given further experimental evidence of the effect of mass ratio on the cylinder response. The Reynolds number used in that work is of order of 10^4, the mass-damping parameter is quite high (between 0.16 and 0.40) and the mass ratio is of order of 10^0. The max amplitude response A^* observed in the experiments is between 0.5 and 1.0, increasing with decreasing mass of the cylinder. In those conditions and with those parameters, again there is no clear evidence of distinct upper and lower branches. This effect is explained in that paper by the high mechanical damping of the system, that drives A^* to less than 0.3 quite rapidly with increasing U^*.

Recently, Pigazzini et al. [19] have proposed a single-degree-of-freedom multi-frequency sdof-mf model for the characterization of the vortex shedding lift force. The proposed model splits the hydrodynamic force acting on the cylinder in Morison-like inertia and drag terms [20, 21], conventionally related to the cylinder motion in still water, and three harmonic terms that account for the lift force induced by pure vortex shedding. These harmonics are assumed to have no mutual (Fourier) relationship. Their amplitudes, frequencies and phase lags, which represent the unknown parameters of the model, can be found according to available VIV data in the time domain. The unknown parameters are identified by a parameter identification (PI) procedure that adopts the Levenberg–Marquardt algorithm [22, 23].

In the present work, the problem of a 2D 1-degree-of-freedom (DoF) VIV in cross-flow direction is tackled. The sdof-mf model and the PI, originally proposed in [19], are exploited further, considering additional representative mass ratios. In particular, the mass ratio is varied systematically three times around a reference value whose VIV data are available from experiments [2, 6]. Mass and mechanical damping ratios are assumed small, still with values related to marine engineering applications. For every mass ratio m^* considered, a large number of reduced velocities U^* is taken into account and simulated via CFD to feed the sdof-mf model. The simulations are carried out using an URANS solver available in OpenFOAM, a CFD toolbox [15–19].

From the overall results, it emerges that the proposed sdof-mf model performs very well in the reproduction of the reference data, even in complex cases (m^*, U^*). Specifically for the present study, the model allowed to examine the effect induced on the hydrodynamic forces by different mechanical properties of the system, here the mass ratio m^*. From the analysis conducted, ultra- or sub-harmonic behavior was systematically found, with magnitude of these additional harmonic terms that depends on m^*. In some cases, they became the dominant part of the vortex shedding lift force, in particular at low m^*.

In the following, the problem formulation is introduced in Sect. 2. The proposed sdof-mf model and the related parameter identification strategy are described in Sect. 3. A brief overview of the CFD simulations used to obtain VIV data is given in Sect. 4. The results obtained from the simulations and from the sdof-mf model are discussed thoroughly in Sect. 5. In particular, selected results are presented first to justify/confirm the applicability of the current sdof-mf model. Then, the focus on the effect of the mass ratio, on the response of the cylinder and on the components of the vortex shedding lift force obtained by the force decomposition adopted in the sdof-mf model, is discussed. Eventually conclusions are given.

2 Problem formulation

A 2D circular cylinder with 1-DoF in the direction perpendicular to a uniform and constant background flow is mounted on a linear spring and a weak linear damper. Figure 1 presents a sketch of the considered system. K and H are the spring and linear damper constants. The cylinder mass, diameter and span are M, D and S, respectively.

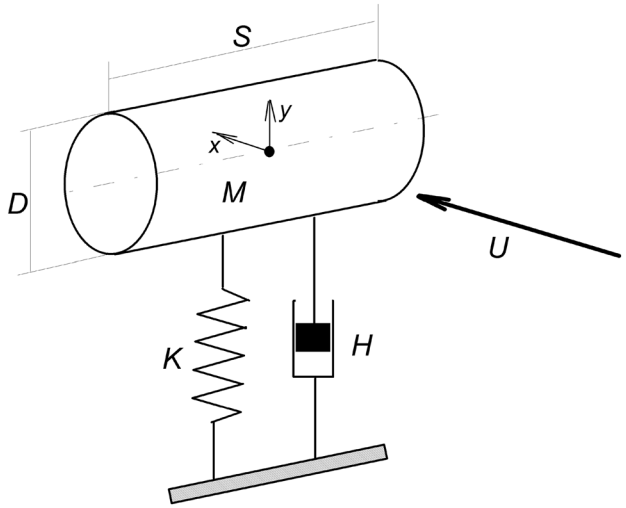

Fig. 1 Schematic representation of VIV problem and relevant symbols

The reduced velocity $U^* = U/(f_0 D)$ and the non-dimensional frequency $f^* = f/f_0$ are introduced as major parameters in VIV, where f is the dominant oscillation frequency of the cylinder, f_0 is the natural frequency of the system in still water and U is the free-stream velocity.

The linear mechanical damping of the system H, used in this study, is such that the damping ratio $\zeta = H/H_{\text{critical}}$ is very low, here $\zeta \approx 5 \times 10^{-3}$. H_{critical} is the standard critical damping of a linear mass-spring-damper system.

The mass M of the cylinder used in the present simulations is such that the problem is characterized by a low mass ratio $m^* = M/(\rho \pi D^2 S/4)$. This parameter is varied systematically three times, still within a practical application range, here $m^* = 1.2,\ 2.4$ and 3.6, starting from a combination of mass, spring stiffness and mechanical damping related to experimental data available in the literature [6]. The value $m^* = 2.4$ is here taken as main reference. It corresponds to the well-known experiments of Khalak and Williamson [6]. Still, further additional experimental data after Govardhan and Williamson [2] are here considered. The analysis is carried out in a parametric way, focusing on the influence of m^* on the fluid–body interaction (fluid forces as proposed by the sdof-mf model) and on the cylinder response.

Tables 1 and 2 give further details, definitions and the full set of parameters of interest.

Table 1 Fixed parameters

Cylinder diameter	D	(m)	3.81×10^{-2}
Cylinder length	S	(m)	2.50×10^{-2}
Cylinder volume	$\nabla = \frac{\pi D^2}{4} S$	(m^3)	2.85×10^{-5}
Spring stiffness	K	$\left(\frac{\text{N}}{\text{m}}\right)$	1.661
Structural damping	H	$\left(\frac{\text{N}}{\text{m/s}}\right)$	4.344×10^{-3}
Potential-added mass	M_A	(kg)	2.847×10^{-2}
Potential-added mass coefficient	$C_\text{A} = \frac{M_\text{A}}{\rho \nabla}$	(–)	1.0
Reynolds number range	Re	(–)	$\approx 0.2/2.7 \times 10^4$

3 Analysis of the results via a proposed sdof-mf model

The mathematical model and parameter identification strategy behind the proposed sdof-mf model have already been presented in Pigazzini et al. [19], here summarized again for sake of completeness.

With reference to Fig. 1 and to Sect. 2, assuming that the cylinder motion is restricted to a single DoF, the rigid body motion equation in still fluid (SF) is:

$$(M + M_\text{A})\,\ddot{y} + H\,\dot{y} + Q\,\dot{y}|\dot{y}| + K\,y = 0. \tag{1}$$

The Morison-like inertia and quadratic drag terms in Eq. 1 constitute the hydrodynamic force in still fluid $F_\text{SF}(t) = -M_\text{A}\,\ddot{y} - Q\,\dot{y}|\dot{y}|$ (the subscript SF here stands for still fluid). In Eq. 1, $M_\text{A} = C_\text{A}\rho(\pi D^2/4)S$ is the added mass, where C_A is the added mass coefficient and $Q = 0.5 C_\text{D} \rho D S$ where C_D is the drag coefficient [20, 21]. The values of added mass and drag coefficients can be estimated according to the Keulegan–Carpenter number of the considered system [20, 21].

In the presence of a background flow with velocity U perpendicular to the DoF above, Eq. 1 is modified to include the additional force that arises from the vortex shedding process, here called $F_\text{VS}(t)$ (the subscript VS here stands for vortex shedding). Thus Eq. 1 is transformed into Eq. 2:

$$(M + M_\text{A})\,\ddot{y} + H\,\dot{y} + Q\,\dot{y}|\dot{y}| + K\,y = F_\text{VS}(t). \tag{2}$$

Assuming that the added mass and drag coefficients are known a priori or from specific tests (free decay or forced oscillations in still fluid), the separation of the total hydrodynamic force $F_\text{TOT}(t) = F_\text{SF}(t) + F_\text{VS}(t)$ in standard inertia/drag and vortex shedding lift terms allows to examine the right-hand side (RHS) of Eq. 2 in details.

As a first approximation, at this stage it is important to point out that the force and/or the response of the cylinder could be assumed almost monochromatic [6]. This is true in most of the U^* range with some exceptions. Nevertheless, a preliminary analysis [19] suggests that the approximation of

Table 2 Varying parameters

Mass ratio	$m^* = \frac{M}{\rho\nabla}$	–	1.2	2.4	3.6
Cylinder mass	M	(kg)	3.42×10^{-2}	6.83×10^{-2}	10.25×10^{-2}
Damping Ratio	$\zeta = \frac{H}{2\sqrt{K(M+M_A)}}$	–	6.734×10^{-3}	5.416×10^{-3}	4.657×10^{-3}
Mass-damping parameter	$m^* \zeta$	–	8.08×10^{-3}	13.00×10^{-3}	16.76×10^{-3}
Modified mass-damp. parameter	$(m^* + C_A)\zeta$	–	14.81×10^{-3}	18.41×10^{-3}	21.42×10^{-3}
Undamped natural frequency in air	$f_{0,a} = \frac{1}{2\pi}\sqrt{\frac{K}{M}}$	(Hz)	1.1100	0.7846	0.6408
Undamped natural frequency in water	$f_0 = \frac{1}{2\pi}\sqrt{\frac{K}{M+M_A}}$	(Hz)	0.8198	0.6592	0.5669

the vortex shedding lift force $F_{VS}(t)$ can be easily and effectively improved considering the contribution of three (at least) harmonics, with the key point that these frequencies are totally independent from each other. In non-dimensional form, $F_{VS}(t)$ can thus be written as

$$\frac{F_{VS}(t)}{F_0} = C_{L,VS}(t) \approx C_{L,VS_{mf}}(t), \tag{3}$$

where the non-dimensional vortex shedding lift force $C_{L,VS_{mf}}(t)$ is written as

$$\begin{aligned} C_{L,VS_{mf}}(t) = &\overline{C_{L,VS_1}} \sin(2\pi \cdot f_{St} \cdot \theta_1 \cdot t + \phi_1) \\ &+ \overline{C_{L,VS_2}} \sin(2\pi \cdot f_{St} \cdot \theta_2 \cdot t + \phi_2) \\ &+ \overline{C_{L,VS_3}} \sin(2\pi \cdot f_{St} \cdot \theta_3 \cdot t + \phi_3). \end{aligned} \tag{4}$$

In Eqs. 3 and 4, the subscript mf stands for the multi-frequency model. $F_0 = \frac{1}{2}\rho DSU^2$ is a reference force and $f_{St} = St \cdot U/D$ is the Strouhal frequency, where St is the Strouhal number.

$\overline{C_{L,VS_i}}$, θ_i and ϕ_i $(i = 1, 3)$ are nine unknown parameters. They are expected to be functions of U^*, m^* and Re. The key point of this sdof-mf model is that frequencies $f_{St} \cdot \theta_i$ $(i = 1, 3)$ in $C_{L,VS_{mf}}(t)$ are assumed not to be Fourier components, thus they are fully uncoupled and not mutually dependent from any Fourier's rule. This assumption allows to build $C_{L,VS_{mf}}(t)$ arbitrarily, with well-identified distinct addends.

Thus, given N_s time-domain samples of the vortex shedding lift force $C_{L,VS}(t_j)$ $(j = 1, N_s)$ and given the corresponding samples of the sdof-mf model $C_{L,VS_{mf}}(t_j)$ $(j = 1, N_s)$, the best-fit sdof-mf model can be found setting the mean square error χ^2 to its minimum, where

$$\chi^2 = \sum_{j=1,N_s} [C_{L,VS}(t_j) - C_{L,VS_{mf}}(t_j)]^2. \tag{5}$$

The best-fit parameters $\overline{C_{L,VS_i}}$, θ_i and ϕ_i, $(i = 1, 3)$ in Eqs. 4 and 5 are found by means of a parameter identification (PI) technique, based on the Levenberg–Marquardt algorithm [22, 23].

As far as the cylinder motion is concerned, the phase lag ψ between the cylinder response and a generic component of the hydrodynamic force takes on some interest. Here, we compute ψ against both $F_{SF}(t)$ and $F_{VS}(t)$ separately. Since the time series of the response and of the forcing terms is in general not monochromatic, we define the phase lag according to the zero-up crossing of the selected signals:

$$\psi = \frac{t_{\text{zero-up}}(y(t)) - t_{\text{zero-up}}(F(t))}{T}. \tag{6}$$

In Eq. 6, $F(t)$ is either $F_{SF}(t)$ or $F_{VS}(t)$, $t_{\text{zero-up}}(y(t))$ and $t_{\text{zero-up}}(F(t))$ are the zero-up crossings of the cylinder motion and force, respectively, and T is the main period of both signals.

4 CFD simulations

As previously described, the current sdof-mf model relies on time-domain VIV data, obtained by simulations or experiments.

In this study, following Pigazzini et al. [19], the VIV data were obtained by CFD simulations using OpenFOAM (*OF*) (release 2.4), an open-source finite-volume-based CFD toolbox. In particular, VIV were obtained with standard URANS simulations. For convenience, full details of the numerical set-up are provided in [19].

At this stage, it is important to clarify that in the former study [19], carried out for $m^* = 2.4$, the URANS simulations predicted an upper branch of A^* whose range in U^* was narrower than the experimental one, i.e. the solution jumped to the lower branch earlier for increasing U^*. In the rest of U^* domain, the main features of the cylinder dynamics were well represented by the simulations, in line with the results reported by other authors using a similar computational URANS-based approach [9–11, 19, 24, 25].

As pointed out in [19], it is worth mentioning that the complexity of the phenomenon (3D nature, detached flow, turbulence, etc.) would probably require more sophisticated and computationally demanding numerical models, mostly

in a narrow range of U^* around the peak of the response of the cylinder.

Aware of the limits of the current CFD approach, this follow-up study aimed to evaluate the effect of the mass ratio within the scope of the sdof-mf model was performed according to [19] for the sake of congruency.

In Figs. 2, 3 and 4, the main features of the cylinder dynamics, corresponding to the three different mass ratios considered in this study, i.e. $m^* = 1.2, 2.4, 3.6$, are compared with the available experimental data and semi-empirical solutions. It is possible to note that in general the numerical results compare well with reference data. Further comments are provided in the following section.

5 Results and discussion

The results obtained using the proposed sdof-mf model are presented as follows. In Sect. 5.1 selected non-dimensional time traces of the vortex shedding force and cylinder displacement are shown to justify the applicability of the current sdof-mf model. Then, the effect of the mass ratio on the cylinder motion and vortex shedding lift force is discussed in Sects. 5.2 and 5.3, respectively.

5.1 Time-domain analysis

The non-dimensional time-domain traces of vortex shedding lift force $F_{VS}(t)$ and cylinder displacement $y(t)$ are shown in Figs. 5 and 6, respectively. More precisely, the time series of $C_{L,VS}(t)$ and $y(t)$ / D obtained via CFD simulations and the current sdof-mf model are compared. As for the time series of $y(t)$ from the sdof-mf model, Eq. 2 has been solved, using Eqs. 3 and 4 for the RHS, adopting a time marching fourth-order Runge–Kutta scheme. The cases proposed in Figs. 5 and 6, in terms of pairs (m^*, U^*), have been selected as highly representative of the U^* dependency of the harmonic content of $C_{L,VS}(t)$ and $y(t)$ / D to justify the applicability of the sdof-mf model. In these figures, solid lines represent CFD time series, whereas dashed lines show sdof-mf time series with best-fit parameters (PI, as described in Sect. 3).

Considering the harmonic content, from Fig. 5a ($m^* = 1.2, U^* = 20$), it is possible to note that a pronounced low frequency oscillation is clearly observed. In this case, the dominant frequencies are f_{St} and $f_{St}/2$.

In Fig. 5b ($m^* = 1.2, U^* = 26$), the dominant frequencies are again f_{St} and $f_{St}/2$, but now they are far enough from

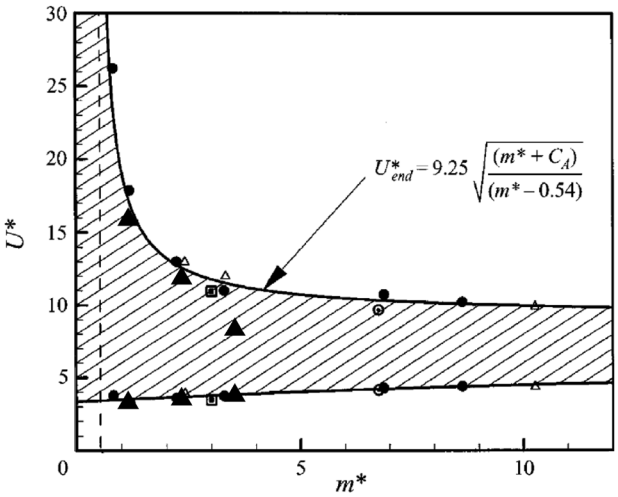

Fig. 3 After Govardhan and Williamson [2]. Range of U^* that embraces the upper and lower branches Vs m^*. (▲) = present numerical, other symbols/lines as in Fig. 5a in [4]

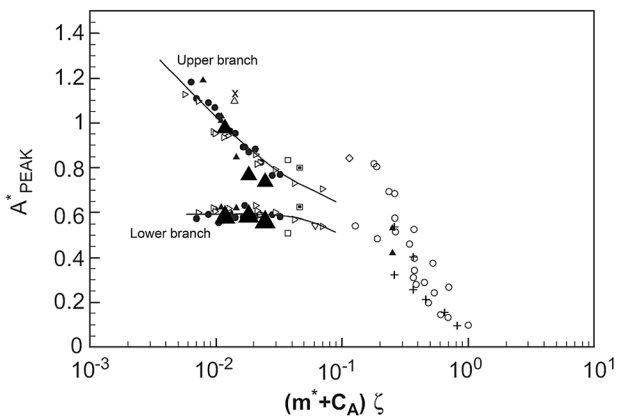

Fig. 2 After Williamson and Govardhan [4]. Maximum value of A^* at the upper and lower branches separately Vs modified mass-damping parameter (see also Tables 1 and 2). (▲) = present numerical; other symbols/lines as in Fig. 6b in [4]

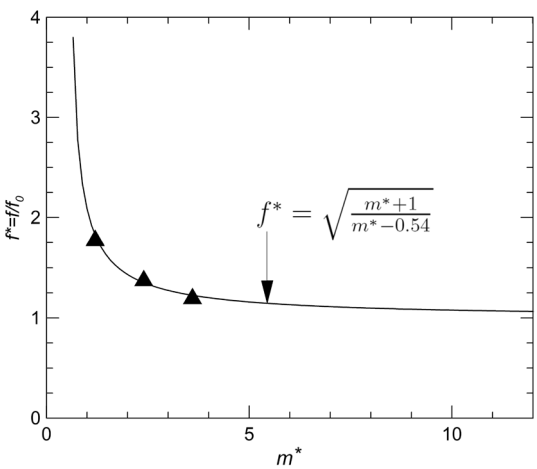

Fig. 4 f^* at lock-in (see Figs. 7b, 8 and 9b) Vs m^*. (▲) = present numerical; solid line = after Williamson and Govardhan [4]

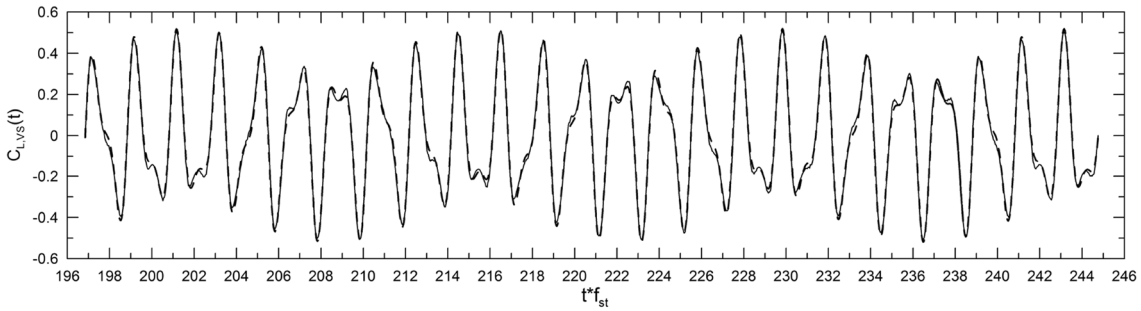

a $m^* = 1.2,\ U^* = 20.00$

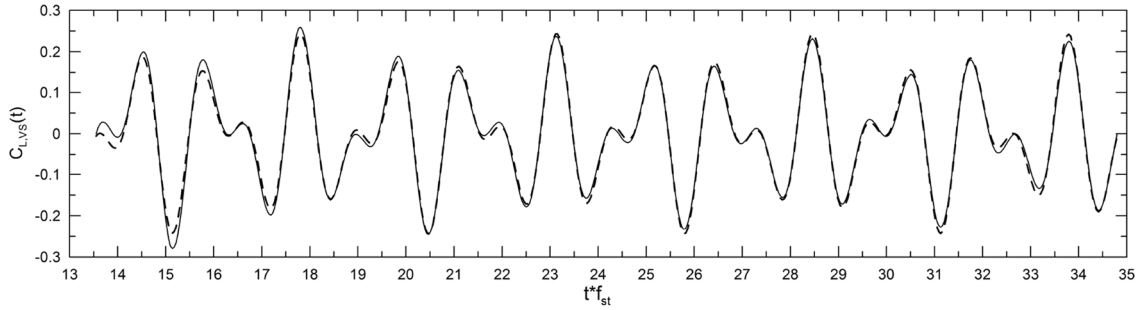

b $m^* = 1.2,\ U^* = 26.00$

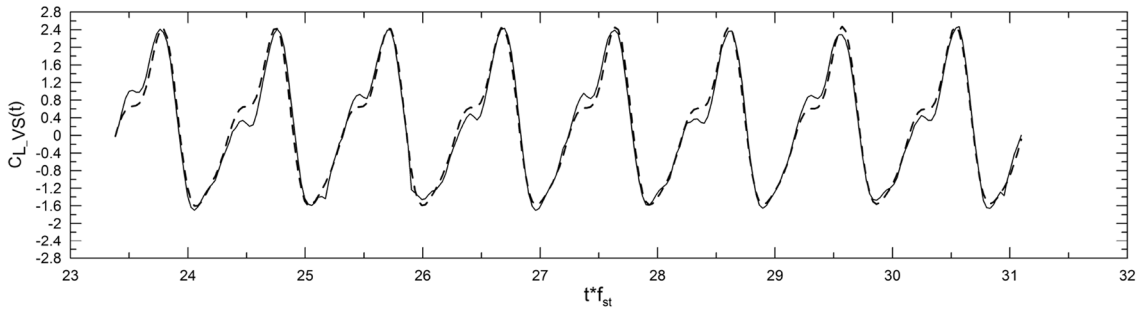

c $m^* = 2.4,\ U^* = 5.35$

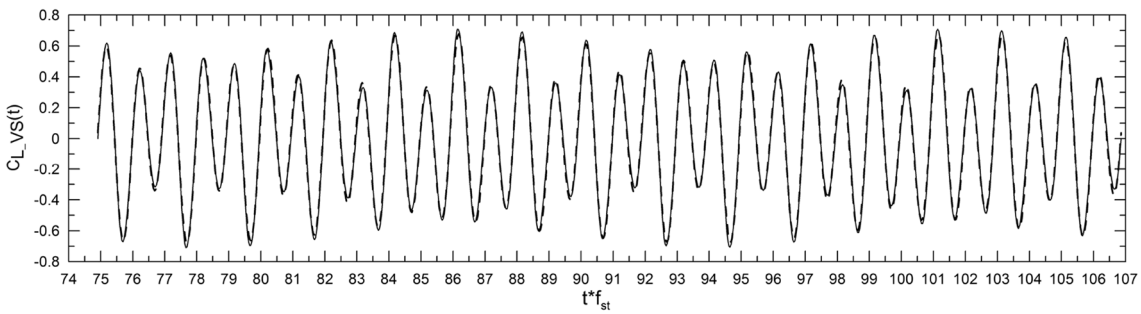

d $m^* = 2.4,\ U^* = 12.50$

Fig. 5 Comparison between time-domain non-dimensional vortex shedding lift force $C_{\mathrm{L,VS}}$ obtained via CFD and via sdof-mf model in Eq. 4. (——) = present CFD; (- - - -) = sdof-mf

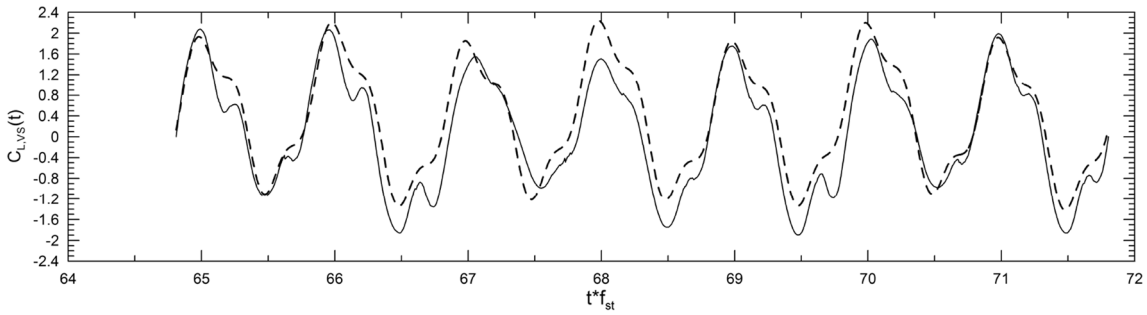

e $m^* = 3.6,\ U^* = 4.75$

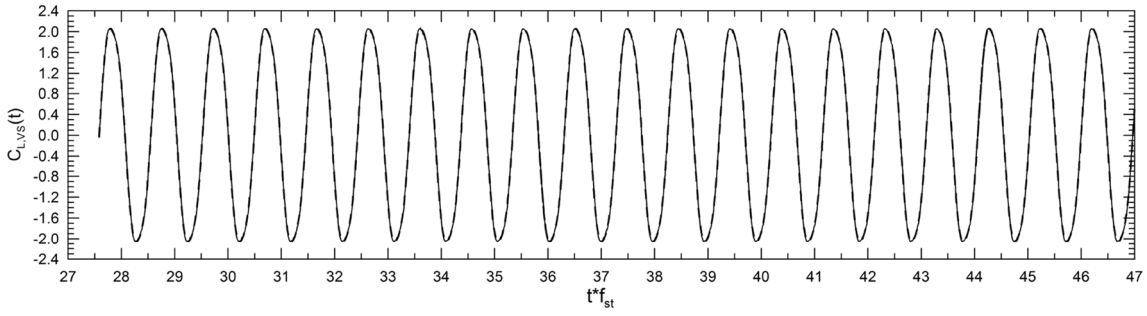

f $m^* = 3.6,\ U^* = 5.95$

Fig. 5 (continued)

each other to lead to a completely different time-domain behavior of $C_{\mathrm{L,VS}}(t)$.

In both cases (Fig. 5a, b), the strongest excitation of the cylinder motion comes from a frequency which is half the conventional Strouhal frequency. In Fig. 5c ($m^* = 2.4$, $U^* = 5.35$), the dominant frequencies are f_{St} and $2 \cdot f_{St}$ approximately.

In Fig. 5d ($m^* = 2.4, U^* = 12.50$), the dominant frequencies are f_{St} and the frequency at lock-in $f^* \approx 1.4$ [6, 14].

In Fig. 5e ($m^* = 3.6, U^* = 4.75$), here used as representative of the worst fit of the sdof-mf model, the harmonic content is very complex and the sdof-mf model, here limited to three harmonics only, lacks additional terms that would probably make the fitting more accurate.

Finally, in Fig. 5f ($m^* = 3.6$, $U^* = 5.95$), the dominant frequencies are f_{St} and $3 \cdot f_{st}$ approximately, though in this case the amplitude of the latter is one order of magnitude smaller than the former.

Summarizing, the proposed sdof-mf model performs very well in the reproduction of the reference data. The fitting of the sdof-mf model is clearly visible, even in complex situations where a multiple harmonic content is dominating the vortex shedding process.

In the following, the effect of the mass ratio on the cylinder motion is presented first. The effect of m^* on the non-dimensional amplitude of the motion, A^*, on the non-dimensional frequency f^* of motion, and on the phase lag ψ (Eq. 6) of the response of the cylinder $y(t)$ Vs $F_{\mathrm{SF}}(t)$ and to $F_{\mathrm{VS}}(t)$, is discussed.

Then, the effect of the mass ratio on the vortex shedding lift force is analyzed. In this case, the characteristic values of the current sdof-mf model, i.e.: $\overline{C_{\mathrm{L,VS}_i}}$ $(i = 1, 3)$ and $(f/f_0)_i = \theta_i \cdot f_{St}/f_0$ $(i = 1, 3)$ are considered.

For the sake of completeness, we remind that the current results were obtained assuming standard values of the added mass/drag coefficients and of the Strouhal number St for subcritical regime, i.e. $C_{\mathrm{A}} = 1.0, C_{\mathrm{D}} = 1.6$ [20, 21] and $St = 0.2$.

5.2 Effect of mass ratio on the cylinder motion

Starting from the motion amplitude, considering Figs. 7a, 8a and 9a, it is possible to note that at the upper branch the maximum value of the non-dimensional amplitude of the cylinder motion, namely A^*_{max}, is achieved for $U^* \approx 5$. Furthermore, A^*_{max} decreases approximately from 0.95 to 0.75, as m^* increases from 1.2 to 3.6. At the lower branch $A^*_{max} \approx 0.6$. With reference to the attitude of the max value of A^* while varying $m^*\zeta$, Williamson and Govardhan [4] presented the results of several research works from the literature. They show the maximum value of A^* at the upper and lower branches separately Vs the modified mass-damping parameter (see also Tables 1 and 2). In Fig. 2, the results of

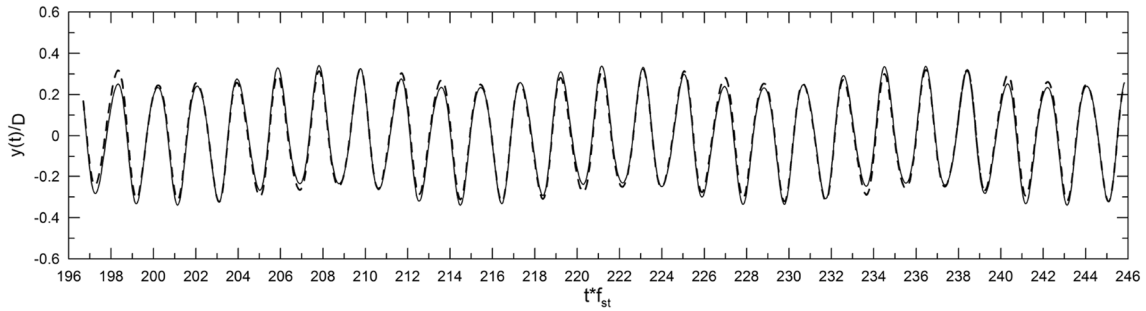

a $m^* = 1.2,\ U^* = 20.00$

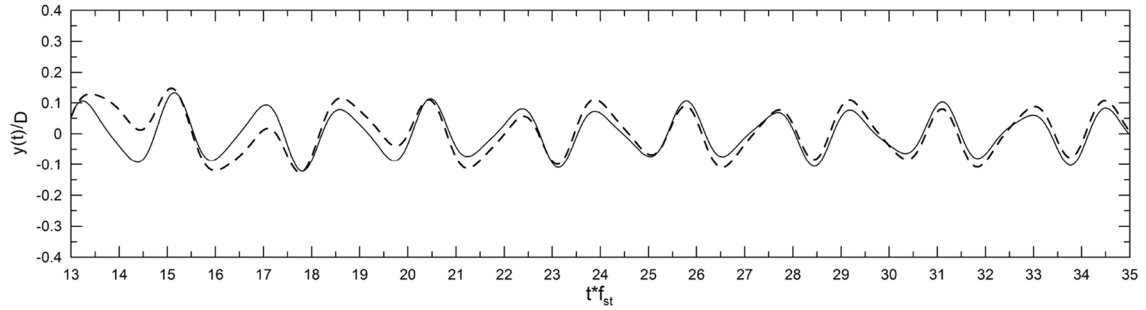

b $m^* = 1.2,\ U^* = 26.00$

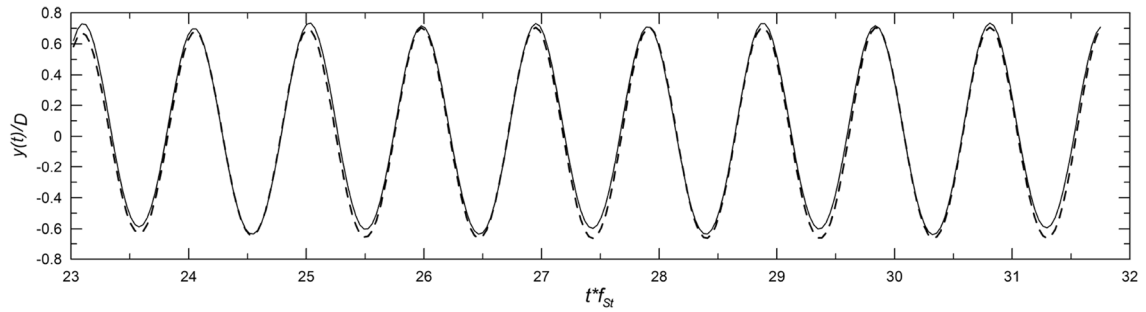

c $m^* = 2.4,\ U^* = 5.35$

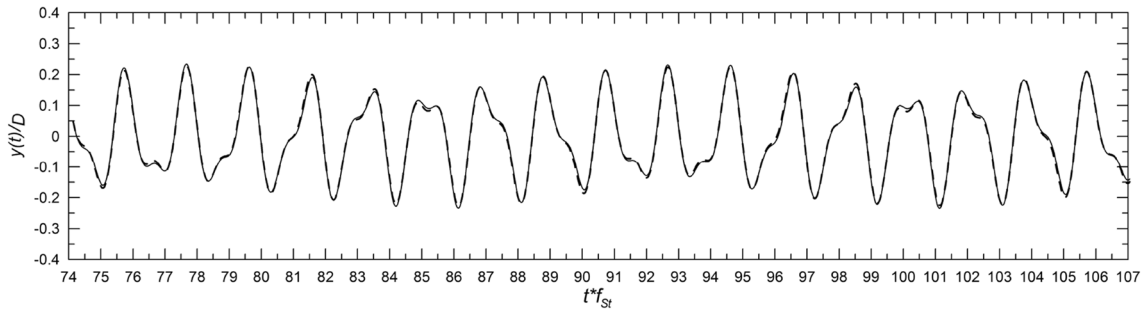

d $m^* = 2.4,\ U^* = 12.50$

Fig. 6 Comparison between time-domain non-dimensional cylinder motion $y(t)$ / D obtained via CFD and via sdof-mf model in Eq. 2. (——) = present CFD; (- - - -) = sdof-mf

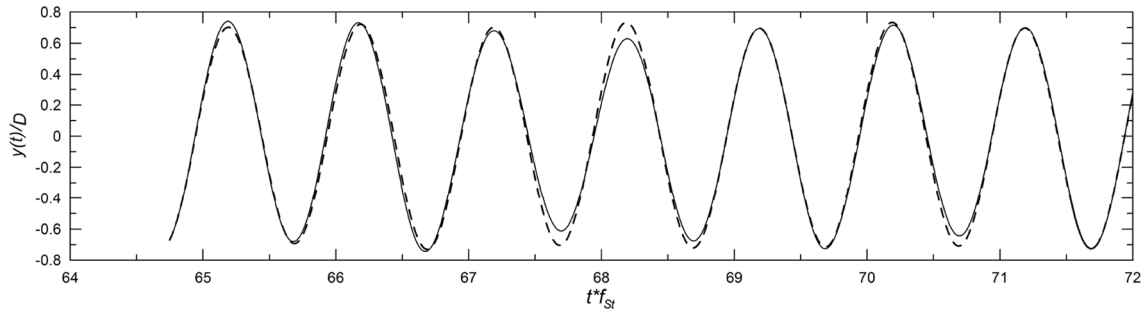

e $m^* = 3.6,\ U^* = 4.75$

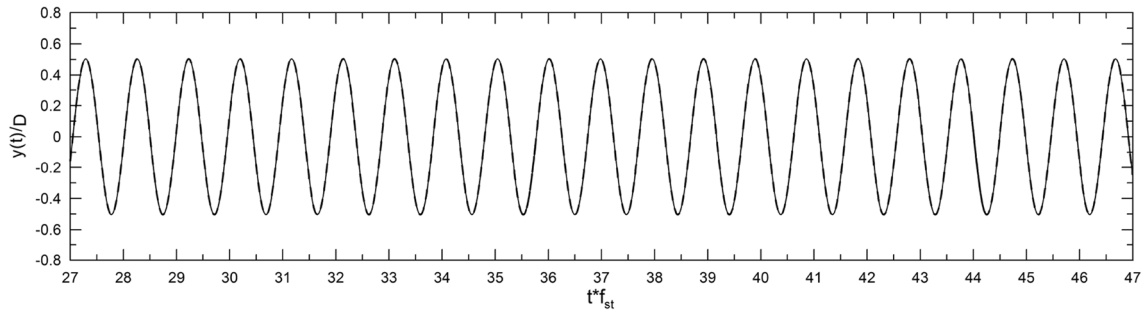

f $m^* = 3.6,\ U^* = 5.95$

Fig. 6 (continued)

the present simulations are compared with the experimental data given by [4]. The upper limit of the lower branch of U^* decreases from $U^* \approx 16$ to $U^* \approx 8$ as m^* increases. From Fig. 3, it is worth noting that the U^* values that embrace upper and lower limits of the lower branches of A^* are in line with the experimental data available in [2]. At the largest values of U^* considered in this study, the order of magnitude of A^* is around 10^{-1}.

Regarding the non-dimensional dominant frequency of the cylinder motion for $m^* = 1.2$, from Fig. 7b it is possible to note that $f^* \approx f_{St}/f_0$ for $U^* < 12$, it turns to $f^* \approx 1.8$ for $12 < U^* < 16$ (right-most part of the lower branch), and then to $0.5 \cdot f_{St}/f_0$ for $U^* > 16$ (sub-harmonic). It is worth mentioning that both the constant value of f^* in the lower branch and the sub-harmonic behavior in desynchronization regime are strongly consistent with the experimental results shown in Fig. 18 of Govardhan and Williamson [2]. For $m^* = 2.4$, in Fig. 8b $f^* \approx f_{St}/f_0$ for $U^* < 5$, it turns to $f^* \approx 1.4$ for $6 < U^* < 13$ (lower branch), and then back to $f^* \approx f_{St}/f_0$ for $U^* > 13$, as clearly shown in the experimental data from Khalak and Williamson [6]. For $m^* = 3.6$, Fig. 9b shows that $f^* \approx f_{St}/f_0$ for $U^* < 5$, it turns to $f^* \approx 1.2$ for $6 < U^* < 8$ (lower branch), and then back to $f^* \approx f_{St}/f_0$ for $U^* > 8$. Eventually, considering Figs. 7b, 8b and 9b it is worth nothing that within the lower branch, the dominant frequency decreases from 1.8 to 1.2 with increasing m^*. Finally, Fig. 4 shows the attitude of f^* at lock-in Vs m^*. The solid line is the function $f^* = \sqrt{(m^* + 1)/(m^* - 0.54)}$ proposed in [2]. Again, the agreement is rather good.

As far as the phase lag ψ between the cylinder response $y(t)$ and $F_{SF}(t)$ is concerned, considering Figs. 7c, 8c and 9c, it is possible to observe an almost in-phase behavior over the entire range of the reduced velocity, as expected. This force is dominated by the inertia term that, for a monochromatic motion, is in anti-phase with the acceleration and thus in phase with the displacement $y(t)$; within the upper and lower branches, the force $F_{SF}(t)$ lags the displacement by approx. 30°. Furthermore, the phase lag ψ between the cylinder response $y(t)$ and the vortex shedding lift force $F_{VS}(t)$ shows a step-like (resonance) behavior with a sharp jump of 165° approx. at $U^* \approx 5$, for the different mass ratios, with $\psi \to 180°$ as U^* increases further.

5.3 Effect of mass ratio on the vortex shedding lift force

As far as the vortex shedding lift force is concerned Figs. 7d, 8d and 9d show that the maximum value of $\overline{C_{L,VS_i}}$ lies between 2.4 and 2.6 for the considered mass ratios. The magnitude decreases slightly with increasing m^*. The value of $U^{*,max}$ at which $\overline{C_{L,VS_i}}$ is maximum, decreases considerably as m^* increases, namely $U^{*,max} \approx 8$, 6.5, 5

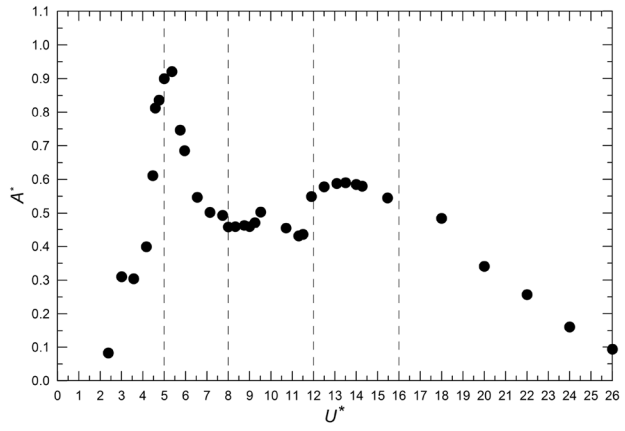

a

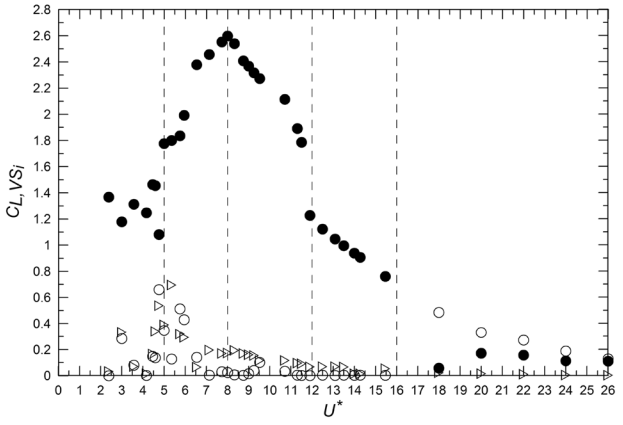

d

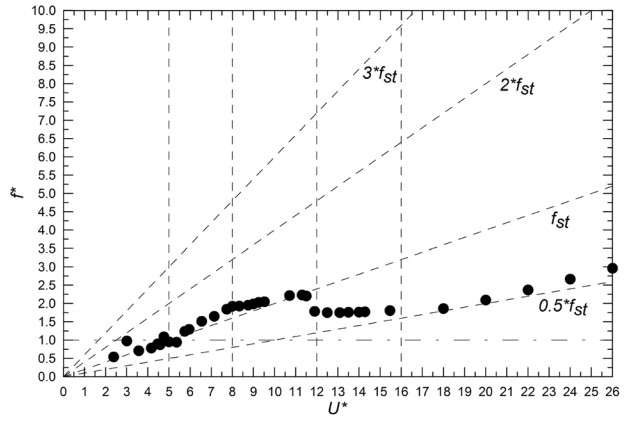

b

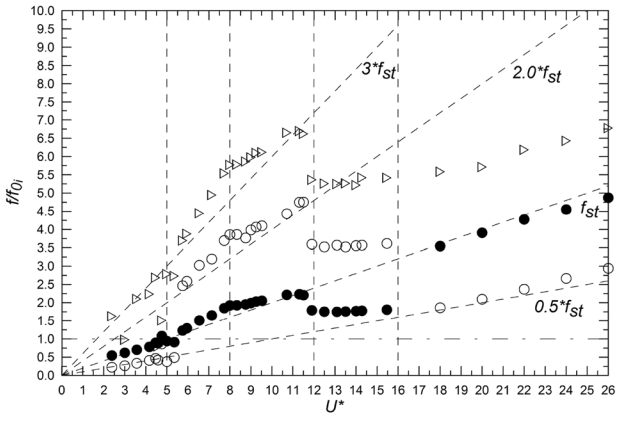

e

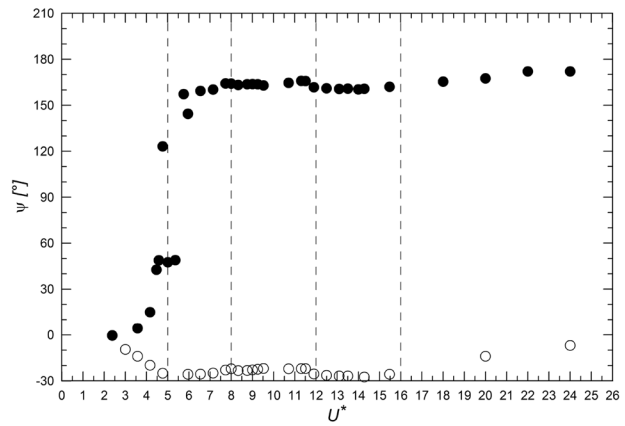

c

Fig. 7 Mass ratio $m^* = 1.2$. **a** Amplitude ratio $A^* = A/D$ and **b** dominant frequency ratio $f^* = f/f_0$ of the cylinder motion Vs $U^* = U/(f_0 \cdot D)$. **c** Phase lag ψ (Eq. 6) of cylinder motion Vs U^*. **d** Vortex shedding lift coefficients $C_{\mathrm{L,VS}_i}$ and **e** frequencies $(f/f_0)_i = \theta_i \cdot f_{St}/f_0$, $i = 1, 3$ of the sdof-mf model Vs U^*. In **b** and **e** oblique dashed lines correspond to $0.5 \cdot f_{St}, 1 \cdot f_{St}, 2 \cdot f_{St}$ and $3 \cdot f_{St}$, where f_{St} is the nominal Strouhal frequency. In **c**, (∘) correspond to the phase lag between the cylinder response $y(t)$ and the Morison-like force $F_{\mathrm{SF}}(t)$, (•) correspond to the phase lag between the cylinder response $y(t)$ and the vortex shedding lift force $F_{\mathrm{VS}}(t)$. In **d** and **e**, (•) are data related to the frequency f^* closest to the Strouhal frequency, $\forall U^*$; for this, m^* (∘) are related to data close to $0.5 \cdot f_{St}$ or $2 \cdot f_{St}$, depending on U^*; (▷) are related to data close to $3 \cdot f_{St}$

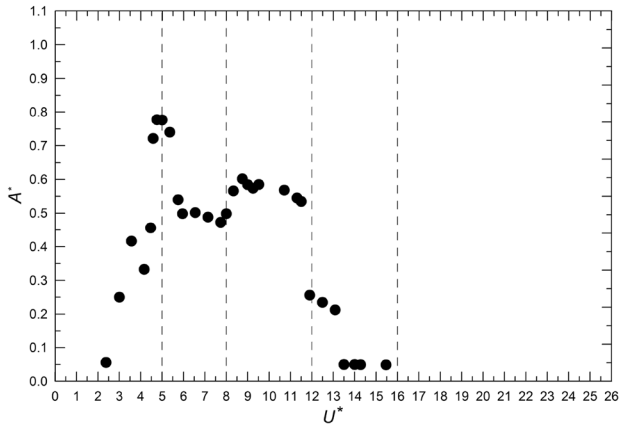

a

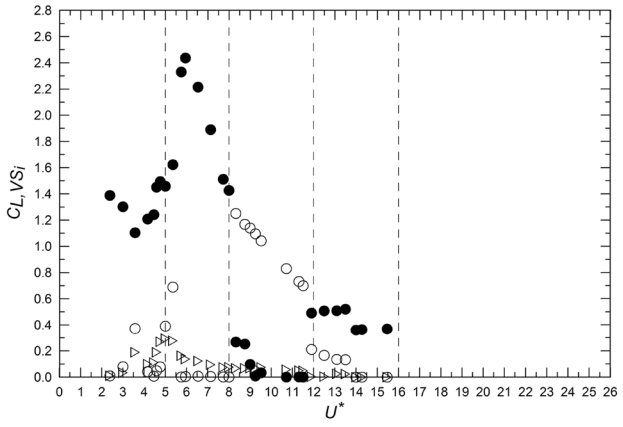

d

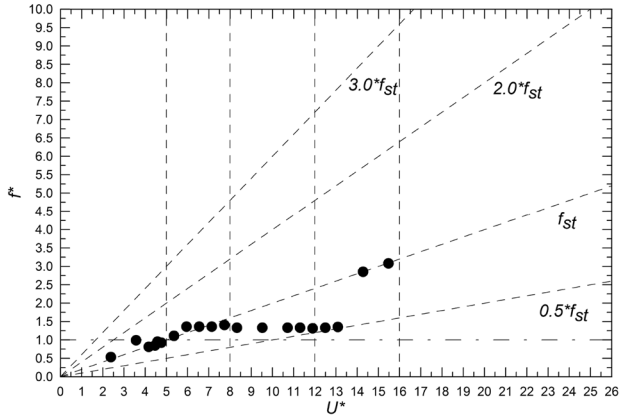

b

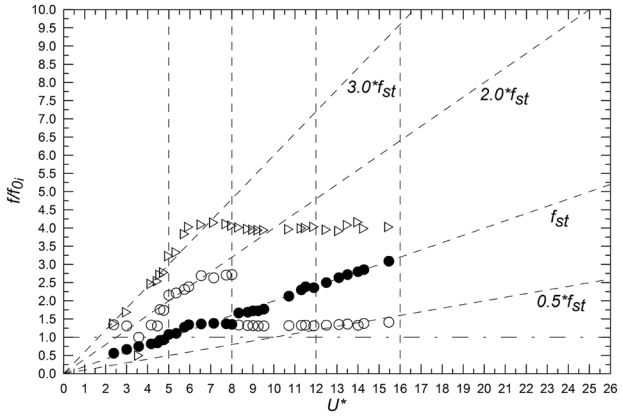

e

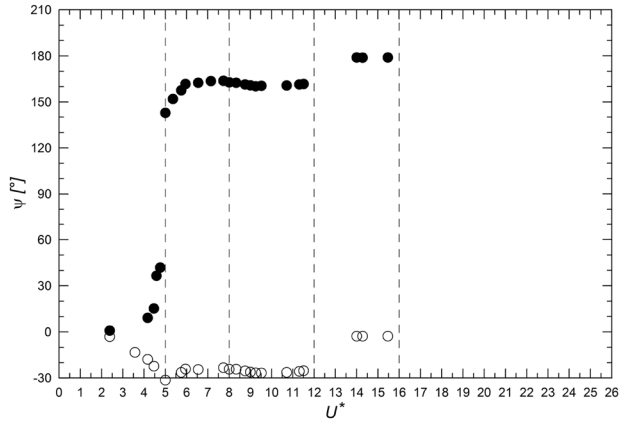

c

Fig. 8 Mass ratio $m^* = 2.4$. **a** Amplitude ***ratio $A^* = A/D$ and **b** dominant frequency ratio $f^* = f/f_0$ of the cylinder motion Vs $U^* = U/(f_0 \cdot D)$. **c** Phase lag ψ (Eq. 6) of cylinder motion Vs U^*. **d** Vortex shedding lift coefficients $\overline{C_{\mathrm{L,VS}_i}}$ and **e** frequencies $(f/f_0)_i = \theta_i \cdot f_{St}/f_0, i = 1, 3$ of the sdof-mf model Vs U^*. In **b** and **e**, oblique dashed lines correspond to $0.5 \cdot f_{St}, 1 \cdot f_{St}, 2 \cdot f_{St}$ and $3 \cdot f_{St}$, where f_{St} is the nominal Strouhal frequency. In **c**, (∘) corresponds to the phase lag between the cylinder response $y(t)$ and the Morison-like force $F_{\mathrm{SF}}(t)$; (•) corresponds to the phase lag between the cylinder response $y(t)$ and the vortex shedding lift force $F_{\mathrm{VS}}(t)$. In **d** and **e**, (•) is data related to the frequency f^* closest to the Strouhal frequency, $\forall U^*$; for this m^* (∘) is related to data close to $2 \cdot f_{St}$ or $1.4 \cdot f_0$, depending on U^*; (⊳) is related to data close to $3 \cdot f_{St}$ and $4.2 \cdot f_0$, depending on U^*

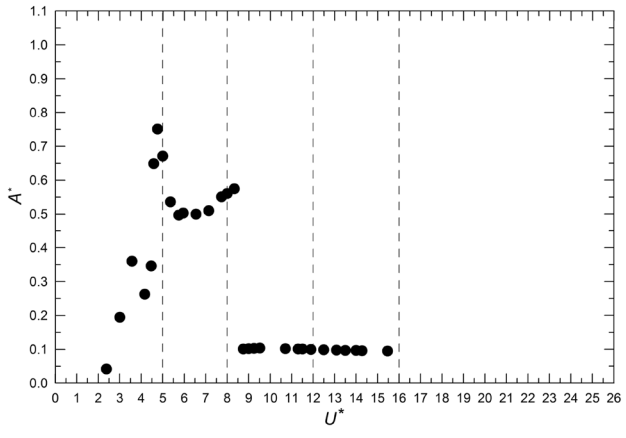

a

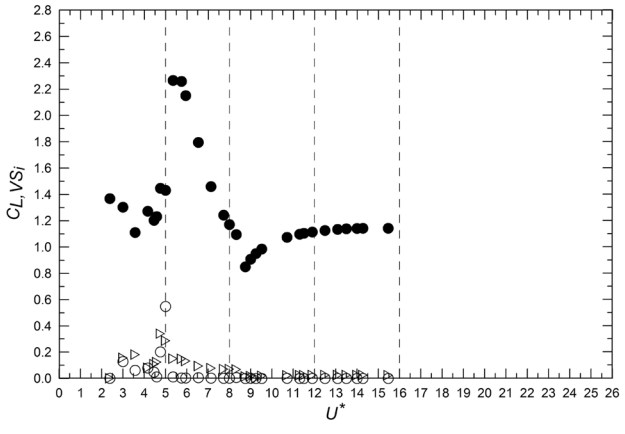

d

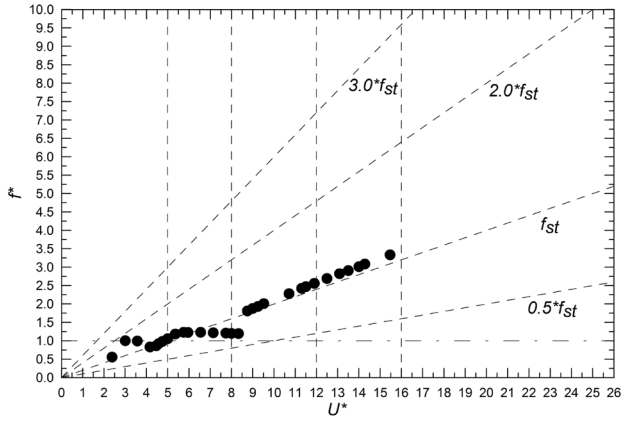

b

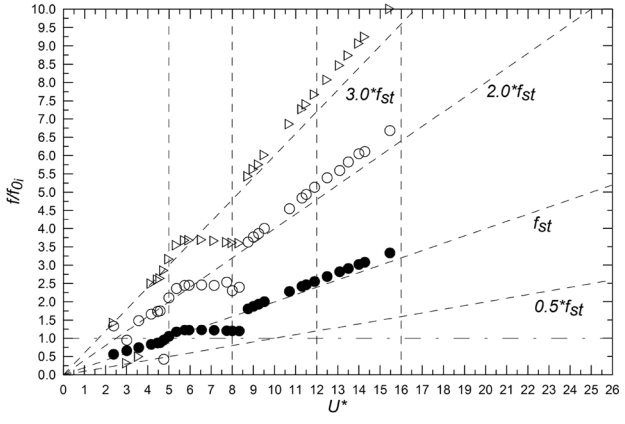

e

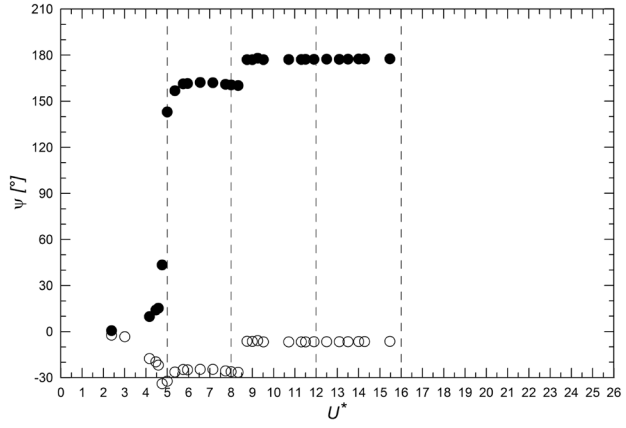

c

Fig. 9 Mass ratio $m^* = 3.6$. **a** Amplitude ratio $A^* = A/D$ and **b** dominant frequency ratio $f^* = f/f_0$ of the cylinder motion Vs $U^* = U/(f_0 \cdot D)$. **c** Phase lag ψ (Eq. 6) of cylinder motion Vs U^*. **d** Vortex shedding lift coefficients $\overline{C_{\mathrm{L,VS}_i}}$ and **e** frequencies $(f/f_0)_i = \theta_i \cdot f_{St}/f_0, i = 1, 3$ of the sdof-mf model Vs U^*. In **b** and **e** oblique dashed lines correspond to $0.5 \cdot f_{St}, 1 \cdot f_{St}, 2 \cdot f_{St}$ and $3 \cdot f_{St}$, where f_{St} is the nominal Strouhal frequency. In **c**, (○) corresponds to the phase lag between the cylinder response $y(t)$ and the Morison-like force $F_{\mathrm{SF}}(t)$; (•) corresponds to the phase lag between the cylinder response $y(t)$ and the vortex shedding lift force $F_{\mathrm{VS}}(t)$. In **d** and **e**, (•) is data related to the frequency f^* closest to the Strouhal frequency, $\forall U^*$; for this m^* (○) is related to data close to $2 \cdot f_{St}$; (▷) is related to data close to $3 \cdot f_{St}$

for $m^* = 1.2,\ 2.4,\ 3.6$, respectively; this is also consistent with the shift, towards lower values, of the upper limit of the range of U^* corresponding to the upper branch (see Fig. 2). Moreover, we point out that for all the investigated mass ratios, the maximum $\overline{C_{\mathrm{L,VS}_i}}$ is related to the frequency closest to the Strouhal frequency, i.e. $(f/f_0)_i \approx f_{St}/f_0$ (typically for $i = 1$). The maximum magnitude of the second harmonic term (i.e. $2 \cdot f_{St}$) in the initial branch is found to be $\overline{C_{\mathrm{L,VS}_i}} \approx 0.6$, of order of 50% of the magnitude at the dominant frequency f_{St}. The third harmonic of $F_{\mathrm{VS}}(t)$ shows up at lock-in, mostly at $5 < U^* < 8$, with amplitudes of $\overline{C_{\mathrm{L,VS}_i}}$, $i = 3$ of order of 10% (or higher) of the dominant term.

Considering Figs. 7e, 8e and 9e, it is possible to note that the non-dimensional dominant frequency $(f/f_0)_i$ of $F_{\mathrm{VS}}(t)$ at lock-in converges to 1 as m^* increases, $(f/f_0)_i \approx 1.8,\ 1.4,\ 1.2$ for $m^* = 1.2,\ 2.4,\ 3.6$, respectively; this is also consistent with the dominant frequency of the cylinder motion (see Fig. 4).

Next the influence of the mass ratio on the value of the dominant term of $F_{\mathrm{VS}}(t)$ is discussed.

From Figs. 7d, e related to $m^* = 1.2$, it is possible to observe that the dominant term of $F_{\mathrm{VS}}(t)$ is found for $U^* < 12$ at $(f/f_0)_i \approx f_{St}/f_0$; for $12 < U^* < 16$ (lower branch) at $(f/f_0)_i \approx 1.8$; for $U^* > 16$, it shows a distinct frequency at exactly half the nominal Strouhal frequency (sub-harmonic) $(f/f_0)_i \approx 0.5 \cdot f_{St}/f_0$, consistently with the dominant frequency of the cylinder motion at large U^* values (see Fig. 7b and the experimental results presented in Fig. 8 of Govardhan and Williamson [2]).

In the case of $m^* = 2.4$, Figs. 8d, e show that the dominant term of $F_{\mathrm{VS}}(t)$ for $U^* < 7$ is found at $(f/f_0)_i \approx f_{St}/f_0$; for $7 < U^* < 12$ at $(f/f_0)_i \approx 1.4$, even though the Strouhal frequency is clearly present, in particular for $8 < U^* < 9$; for $U^* > 12$ the nominal Strouhal frequency takes the control of the forcing term again.

For $m^* = 3.6$, Figs. 9d, e show that the dominant term of $F_{\mathrm{VS}}(t)$ for $U^* < 5.5$ is found at $(f/f_0)_i \approx f_{St}/f_0$; for $5.5 < U^* < 8.5$, at $(f/f_0)_i \approx 1.2$; for $U^* > 8.5$, the nominal Strouhal frequency takes the control of the forcing term again.

From the results, it emerges that ultra- or sub-harmonic behavior is systematically found, with magnitude of these additional harmonic terms that depend on the mass ratio m^*. In some cases, they become the dominant part of the vortex shedding lift force. In particular at low m^*, the typical sharp drop of A^* between the lower branch and the desynchronization regime disappears, and a dominant sub-harmonic term in both motion and vortex shedding lift force is observed; for increasing U^*, this sub-harmonic frequency keeps the control of the system, it grows almost linearly and correspondingly A^* decreases slowly.

6 Concluding remarks

Vortex-induced vibrations (VIV) of an elastically-mounted 2D circular cylinder in cross-flow, with low mass and damping ratios, were studied varying systematically the mass ratio m^* of the system, within a range of interest for practical engineering applications in water.

The study was carried out using a single-degree-of-freedom-multi-frequency (sdof-mf) model, where the total hydrodynamic force acting on the cylinder is split in conventional Morison-like inertia/drag terms with standard added mass and drag coefficients, and three harmonics that account for the vortex-induced lift force. A parameter identification (PI) method, applied in the time domain to available VIV data, allows to obtain the unknown model parameters, i.e. amplitudes, frequencies and phases of the three harmonics.

In this study, the VIV data used in the coupled sdof-mf/PI approach were obtained by URANS simulations, keeping the same CFD framework already used in a previous work.

From the overall results, it emerges that the sdof-mf model reproduces the time-domain cylinder motion and vortex shedding lift force quite accurately. The parameters of the sdof-mf model show a fair and consistent variation over the entire range of U^* and for all m^*.

The systematic application of the sdof-mf model provides a rather deep insight in the characterization of the vortex-induced lift force. In particular, the main outcome of the analysis of this force is found in the presence of ultra- and sub-harmonic terms. For specific pairs (U^*, m^*), these ultra- and sub-harmonic terms are observed to take the control of the VIV process, both at lock-in and in desynchronization regions.

Acknowledgements The Regional Program POR FESR 2014 2020-1.3.b-Ricerca e sviluppo-Aree tecnologie marittime e smart health of the Regione Friuli-Venezia Giulia is acknowledged for providing the financial support of the SOPHYA Project. The Scholarship co-funded by the EUROPEAN SOCIAL FUND, Axis 3 EDUCATION AND TRAINING, OPERATION ESF S3: Scholarships in FRIULI VENEZIA GIULIA is also acknowledged.

References

1. Bearman P (1984) Vortex shedding from oscillating bluff bodies. Ann Rev Fluid Mech 16(1):195–222
2. Govardhan R, Williamson C (2000) Modes of vortex formation and frequency response of a freely vibrating cylinder. J Fluid Mech 420:85–130. https://doi.org/10.1017/S0022112000001233
3. Gabbai R, Benaroya H (2005) An overview of modeling and experiments of vortex-induced vibration of circular cylinders. J Sound Vib 282:575–616. https://doi.org/10.1016/j.jsv.2004.04.017

4. Williamson C, Govardhan R (2008) A brief review of recent results in vortex-induced vibrations. J Wind Eng Ind Aerodyn 96:713–735. https://doi.org/10.1016/j.jweia.2007.06.019
5. Bearman P (2011) Circular cylinder wakes and vortex-induced vibrations. J Fluids Struct 27:648–658. https://doi.org/10.1016/j.jfluidstructs.2011.03.021
6. Khalak A, Williamson C (1996) Dynamics of a hydroelastic cylinder with very low mass and damping. J Fluids Struct 10(5):455–472. https://doi.org/10.1006/jfls.1996.0031
7. Vikestad K, Vandiver J, Larsen C (2000) Added mass and oscillation frequency for a circular cylinder subjected to vortex-induced vibrations and external disturbance. J Fluids Struct 14:1071–1088. https://doi.org/10.1006/jfls.2000.0308
8. Norberg C (2003) Fluctuating lift on a circular cylinder: review and new measurements. J Fluids Struct 17:57–96. https://doi.org/10.1016/S0889-9746(02)00099-3
9. Guilmineau E, Queutey P (2004) Numerical simulation of vortex-induced vibration of a circular cylinder with low mass-damping in a turbulent flow. J Fluids Struct 19(4):449–466. https://doi.org/10.1016/j.jfluidstructs.2004.02.004
10. Wanderley J, Souza G, Sphaier S, Levi C (2008) Vortex-induced vibration of an elastically mounted circular cylinder using an upwind TVD two-dimensional numerical scheme. Ocean Eng 35(14):1533–1544. https://doi.org/10.1016/j.oceaneng.2008.06.007
11. Wu W, Bernitsas MM, Maki K (2014) RANS simulation versus experiments of flow induced motion of circular cylinder with passive turbulence control at $35,000 < RE < 130,000$. J Offshore Mech Arct Eng 136(4):041802
12. Mittal N, Mittal S (2016) Lock-in in vortex-induced vibration. J Fluid Mech 794:565–594. https://doi.org/10.1017/jfm.2016.157
13. Bahmani MH, Akbari MH (2010) Effects of mass and damping ratios on VIV of a circular cylinder. Ocean Eng 17:511–519. https://doi.org/10.1016/j.oceaneng.2010.01.004
14. Modir A, Kahrom M, Farshidianfar A (2016) Mass ratio effect on vortex induced vibration of a flexibly mounted circular cylinder, an experimental study. J Mar Energy 16:1–11. https://doi.org/10.1016/j.ijome.2016.05.001
15. Contento G, Lupieri G, Jasak H, Vukčević V (2015) Numerical study of unsteady breaking waves induced by a submerged hydrofoil at steady forward speed. In: NAV 2015 18th international conference on ships and shipping research
16. Lupieri G, Contento G (2015) Numerical simulations of 2-D steady and unsteady breaking waves. Ocean Eng 106:298–316. https://doi.org/10.1016/j.oceaneng.2015.07.014
17. Morgut M, Jošt D, Nobile E, Škerlavaj A (2015) Numerical investigation of the flow in axial water turbines and marine propellers with scale-resolving simulations, 33rd UIT (Italian Union of Thermo-fluiddynamics) Heat Transfer Conference. J Phys Conf Ser 655:12–52. https://doi.org/10.1088/1742-6596/655/1/012052
18. Lupieri G, Contento G (2017) On the wavy flow past a weakly submerged horizontal circular cylinder at low Keulegan–Carpenter numbers. J Mar Sci Technol 22(4):673–693. https://doi.org/10.1007/s00773-017-0445-y
19. Pigazzini R, Contento G, Martini S, Puzzer T, Morgut M, Mola A (2018) VIV analysis of a single elastically-mounted 2D cylinder: parameter identification of a single-degree-of-freedom multi-frequency model. J Fluids Struct 78:299–313. https://doi.org/10.1016/j.jfluidstructs.2018.01.005
20. Sarpkaya T, Isaacson M (1981) Mechanics of wave forces on offshore structures. Van Nostrand Reinhold, New York
21. Morison J, O'Brien M, Johnson J, Schaaf S (1950) The force exerted by surface waves on piles. Petrol Trans 189:149–154. https://doi.org/10.2118/950149-G
22. Levenberg K (1944) A method for the solution of certain nonlinear problems in least squares. Quart Appl Math 2(2):164–168
23. Marquardt D (1963) An algorithm for the least-squares estimation of nonlinear parameters. J Soc Ind Appl Math 11(2):431–441
24. Kinaci OK (2016) 2-D URANS simulations of vortex induced vibrations of circular cylinder at Trsl3 flow regime. J Appl Fluid Mech 9(5):2537–2544
25. Pan Z, Cui W, Miao Q (2007) Numerical simulation of vortex-induced vibration of a circular cylinder at low mass-damping using RANS code. J Fluids Struct 23(1):23–37